




Maiolica seen by Vis–NIR hyperspectral imaging spectroscopy: the application of an ultraportable camera at the Museo Nazionale del Bargello

Francesca Galluzzi^{1,a}, Rosarosa Manca^{2,b} , Massimiliano Puntin^{3,c}, Simona Raneri^{4,d}, Claudia Sciuto^{3,e}, Marco Benvenuti^{2,5,f}, Rémy Chapoulie^{1,g}

¹ Archéosciences Bordeaux UMR 6034, CNRS, Université Bordeaux Montaigne, Pessac, France

² Earth Sciences Department, Università degli Studi di Firenze, Via La Pira 4, 50121 Florence, Italy

³ MAPP Lab, Department of Civilizations and Forms of Knowledge, University of Pisa, Pisa, Italy

⁴ CNR-ICCOM, Pisa, Italy

⁵ CNR-IGG, Florence, Italy

Received: 19 December 2023 / Accepted: 27 June 2024

© The Author(s) 2024

Abstract An ultraportable hyperspectral camera operating in the Vis–NIR range (400–1000 nm) was used in this study for the non-invasive analysis of a selection of Italian maiolica wares and sherds from the Museo Nazionale del Bargello in Florence, Italy. The studied objects included authentic archaeological sherds, nineteenth-century forgeries, and ceramics of uncertain origin. The primary aim of this study was to evaluate the efficacy of hyperspectral imaging (HSI) spectroscopy combined with multivariate analysis for examining highly refractive and three-dimensional glazed ceramic artefacts within the constraints of a museum environment, including imperfect lighting conditions. Two data processing pipelines were tested: one based on principal component analysis (PCA) with score plots and the other on spectral angle mapper (SAM) classification obtained through the ENVI Spectral Hourglass Wizard (ENVI-SHW). The analyses enabled the discrimination between original parts and/or restored parts and additions. Among others, a complex assemblage of original sherds, restored parts, and non-ceramic parts was observed in a Renaissance pastiche vase. Furthermore, the method enabled the identification of the various chromophores providing clues on the artistic colour palette. In particular, the identification of chromium in the blue and green glazes of two objects of uncertain chronology suggested that they were not made before the nineteenth century. The acquisition of a larger and more detailed database of HSI data on maiolica glazes is strongly encouraged to improve the applicability of this method in authenticity, art-historical and archaeological studies.

1 Introduction

The collections of glazed ceramics held in museums represent an immense source of information about the socio-cultural context in which they were produced, providing clues on the manufacturing techniques, the artistic taste, and the trade connections. Moreover, each object has an individual history that includes uses, re-contextualization and restoration. It is not always possible to keep track of all these trajectories, and often, the only source for reconstructing the histories of objects is the study of their material characteristics. When analysing these objects, non-invasive and portable techniques are frequently the preferred methods and, sometimes, the only viable ones. This approach helps safeguard the object's integrity and enables in situ, repeatable analyses, making it possible to study fragile objects with minimal handling.

In these perspectives, Vis–NIR hyperspectral imaging (HSI) spectroscopy (400–1000 nm) presents several advantages since: (i) it allows performing non-invasive and contactless analysis; (ii) highly portable cameras are available; (iii) there are no health and safety constraints, such as those linked to ionising radiation; (iv) the acquisition of data is fast and easy, thus allowing the screening of large areas and a high number of objects [1]. For decorated surfaces, HSI enables the characterisation and the mapping of artistic materials and the localisation of differences in polychromatic patterns. For each pixel in the acquired image, reflectance spectra at different wavelengths are recorded. However, the acquisition of an extensive hyperspectral data cube requires multivariate analysis

^a e-mail: francesca.galluzzi@u-bordeaux-montaigne.fr

^b e-mail: rosarosa.manca@unifi.it (corresponding author)

^c e-mail: massimiliano.puntin@gmail.com

^d e-mail: simona.raneri@pi.iccom.cnr.it

^e e-mail: claudia.sciuto@unipi.it

^f e-mail: m.benvenuti@unifi.it

^g e-mail: remy.chapoulie@u-bordeaux-montaigne.fr

for data reduction and extraction of relevant information. An increasing number of data processing routines have been developed and employed to enhance data visualisation and classification while reducing computation time [2–5]. Reflectance imaging spectroscopy has been extensively used to analyse a wide range of polychromatic objects, including mural [6, 7] and canvas [8, 9] paintings, textiles [10, 11], manuscripts [12, 13], prints [14, 15] and historical glasses [16, 17], with a general preference for artefacts having flat surfaces [18], since this aspect facilitates the acquisition and treatment of the images. In particular, the portable Specim IQ camera has proven to be effective in recent cultural heritage applications within art history and archaeology in the field and in museums [1, 2, 19]. However, only a few applications of HSI on glazed pottery have been reported in the literature and, to the author's knowledge, none of them concerns Italian maiolica. For example, Beauvoit et al. applied HSI on polychrome glazed ceramics from the Vieillard & Co factory in France [20], while Sciuto et al. studied Iznik ceramic tiles [1]. Infrared false-colour (IRFC) photography has been used in maiolica studies [21], while fibre optics reflectance spectroscopy (FORS) in the UV–Vis and Vis–SWIR range have been implemented in the investigation of enamels [22], ceramic materials [23, 24], mosaic tesserae [25], and ceramic tiles with a lead-based glaze [26]. In this study, we propose the use of an ultraportable HSI camera (Specim IQ) operating in the Vis–NIR range (400–1000 nm) for the study of a selection of Italian maiolica wares and sherds of the Museo Nazionale del Bargello in Florence, Italy.

Maiolica is an Italian word indicating earthenware materials coated with tin-opacified and coloured glazes [27]. This type of pottery developed during the Middle Ages and the Renaissance, becoming an iconic artistic production of these periods in Italy. After about two centuries of decline, maiolica had a revival period in the second half of the nineteenth century, when the previous productions started to be collected, restored, copied, and forged [28–31]. This extensive production makes authentication studies essential for understanding the social and economic context in which the copies were produced. An interpretation of maiolica collections as objects revealing the origin and diffusion of different types of production necessarily uses a scientific approach, which is essential for the description of the biographies of individual objects and entire collections [32]. Furthermore, the outcome of scientific investigations is important in technical art history studies and in planning conservation and preservation treatments.

In these perspectives, this study aimed to explore the potential of HSI in the characterisation of Italian maiolica, with a focus on the discrimination of parts with different compositions within the same object, including restorations and integrations, and the identification of pigments and dyes used over the centuries. The extensive maiolica collection at the Museo Nazionale del Bargello in Florence, Italy, founded in 1865, was a rich resource for the analysis of a wide range of artefacts, from original archaeological sherds to nineteenth-century forgeries. The hyperspectral images were acquired directly in situ. Challenges, such as shadows and scattering effects, were posed by the complex three-dimensional artefacts with highly reflective surfaces. Therefore, another objective of this research was to evaluate appropriate and effective data processing methods to elaborate hyperspectral images of exceptionally reflective surfaces acquired under conditions that diverge from those typically encountered in conventional laboratory settings. To achieve this, two different pipelines were followed independently, and the outcomes were compared. Ultimately, this will contribute to the characterisation of valuable works of art housed in museum collections.

2 Materials and methods

2.1 Maiolica wares and sherds

The maiolica wares and sherds that were analysed by HSI in this study belong to the collection of the Museo Nazionale del Bargello collection in Florence, Italy. The artefacts are shown in Fig. 1 and described in Table 1. These artefacts have been divided into three different groups, namely (a) Italian maiolica made between the thirteenth and the sixteenth century; (b) copies and forgeries of Italian maiolica made between the nineteenth and the twentieth century; and (c) maiolica of uncertain dating and authenticity.

The samples belonging to the first two groups (a and b) were investigated in a previous analytical study [33] using various analytical techniques (see Table 1), while samples from group (c) were not analysed before. More in detail, group (a) consists of 4 sherds from archaeological excavations (samples A_AUT1, B_AUT3, C_AUT2, B_AUT4) and a lustrated tile (581 M). All the samples of group (a) were investigated by X-ray fluorescence spectroscopy (XRF), which allowed the characterisation of the elemental composition of the glaze and the colouring materials. In addition to this, thermoluminescence analysis (TL) confirmed the authenticity of the lustrated tile (C_AUT2), while micro-samples taken from the archaeological sherds were analysed by scanning electron microscopy coupled with energy-dispersive X-ray spectrometry (SEM–EDS) to characterise their composition and layer structure. The *pastiche* vase with the faces of two men in relief (520 M) comprises original Renaissance parts of the sixteenth century (called ‘original parts’ hereafter) and parts manufactured around the end of the nineteenth century to reconstruct the whole object (called ‘modern parts’ hereafter). Original and modern parts are kept together by non-ceramics (plaster) joints. The original Renaissance parts of the *pastiche* vase were classified in group (a), while the ‘modern’ parts were classified in group (b) (Table 1). In this latter group, a pharmacy jar adorned with blue decorations (583 M) was previously identified as a forgery through stylistic observations [30], XRF results, and a TL authentication test [33]. Finally, group (c) comprises three wares of uncertain authenticity, identified as possible forgeries by the museum curator due to stylistic and historical considerations: a plate with peacock-eye decoration (1897 M), a leopard figurine (1838C), and a bowl with a deer (376 M). Note that plate with peacock-eye decoration 1897 M and *pastiche* vase 520 M appear to be made of different parts assembled together probably with painted plaster integrations (see Fig. 1).



Fig. 1 Maiolica wares and sherds of the Museo Nazionale del Bargello (Italy) analysed in this study. Group **a**: authentic Italian maiolica made between the thirteenth and sixteenth centuries. Group **b**: maiolica made between the nineteenth and twentieth centuries. Group **c**: wares of uncertain dating and authenticity

2.2 VIS–NIR HSI image acquisition

HSI measurements were performed using the Specim IQ push-broom hyperspectral camera (SPECIM Spectral Imaging Ltd., Oulu, Finland), which covers the visible light and near-infrared (Vis–NIR) spectral range from 400 to 1000 nm, with 204 spectral bands across the entire wavelength range. The spectral resolution (FWHM) is 7 nm, with an acquisition step of 3.5 nm. The resolution of the resulting image is 512×512 pixels. The ultraportable camera, characterised by a light weight of 1.3 kg and compact dimensions ($207 \times 91 \times 126$ mm), allowed an effortless international transport to the museum, unlike other transportable instruments that may require more specialised logistics. Its capacity to operate effectively at short distances and real-time data acquisition, processing and visualisation under further accentuated its suitability for the analysis. The hyperspectral images were acquired directly inside the museum and under diffuse halogen lighting provided by one single lamp of 300 W. The camera was positioned on a photographic tripod, and the analyses were conducted at a working distance of approximately 0.30 m or less as a function of the object size. The integration time for the analysis was 32 ms. A white Spectralon® standard was employed for HSI data calibration to ensure data accuracy and reliability.

2.3 Image processing

Infrared false-colour (IRFC) images were generated using the ENVI software by substituting an infrared band for the red channel and selecting two other bands in the visible range for the green and blue channels ($R \rightarrow 900$ nm; $G \rightarrow 650$ nm; $B \rightarrow 550$ nm). Two different data processing methods were then applied; principal component analysis (PCA) with score plots and ENVI's 'hourglass paradigm' followed by spectral angle mapper (SAM) classification. In order to observe any possible difference in the results obtained with the two pipelines, they were run independently and then compared. The aim was to assess their effectiveness in studying glazed ceramic samples, which often involve challenges such as light scattering and shadows. Notably, SAM's insensitivity to spectral intensity can be advantageous for analysing hyperspectral images acquired with non-uniform illumination. In contrast, variations in spectral intensity caused by scattering phenomena and shadow zones might significantly limit PCA's ability to analyse such parts of the images [7]. Nevertheless, the PCA images achieved through the score plot might be helpful for screening and identifying outliers, anomalies, or features that SAM may not detect [7, 34].

The acquired data cube was explored through Principal Components Analysis (PCA), an unsupervised dimensionality reduction method that is largely used in the analysis of hyperspectral datasets [7, 35, 36]. Raw spectral data were processed using Prediktera's Evince software, which automatically calculates PCA on registered hyperspectral images. It is noteworthy that PCA models neces-

Table 1 Maiolica wares and sherds of the Museo Nazionale del Bargello analysed in this study

Inv.N.	Description	Date of production	Place of production	Colours	Previous analysis [33]
<i>Group (a)—thirteenth–sixteenth century</i>					
A_AUT1	Sherd of archaic maiolica	Late 13th–14th cent	Orvieto (Italy)	Green, brown	XRF, SEM–EDS
B_AUT3	Sherd with flowers	15th cent., 2nd half	Area of Florence (Italy)	Blue, brown, white	XRF, SEM–EDS
B_AUT4	Sherd of pharmacy jar	15th cent., 2nd half	Deruta (Italy)	Blue, orange, aqua, white, brown	XRF, SEM–EDS
C_AUT2	Sherd with lustre decorations	16th cent	Deruta (Italy)	Lustre, blue, white	XRF, SEM–EDS
581 M	Tile with lustred decorations	15th–16th cent	Gubbio or Valencia (Spain)	Lustre, blue, white	XRF, TL
520 M	<i>Pastiche</i> vase with faces in relief—Renaissance parts	16th cent	Central Italy	Blue, orange, brown, green, white	XRF
<i>Group (b)—nineteenth–twentieth century</i>					
520 M	<i>Pastiche</i> vase with faces in relief—19th–20th-century parts	19th–20th cent	Central Italy (before 1934)	Blue, yellow, brown, green, white/pink	XRF
582 M	Pharmacy jar with dog	19th–20th cent	Central Italy, possibly Faenza	Blue, orange, green, white	XRF, TL
<i>Group (c)—Uncertain authenticity</i>					
1897 M	Dish with peacock-eye decoration (with restored rim)	Unknown	Unknown	Blue, orange, white	None
1838 C	Leopard figurine	Unknown	Unknown	Blue, yellow, white	None
376 M	Bowl with deer	Unknown	Unknown	Green, brown, yellow, white	None

Previous analyses were performed by Manca et al. [33]. XRF = X-ray fluorescence spectroscopy. TL = Thermoluminescence analysis. SEM–EDS = Scanning electron microscopy coupled with energy-dispersive spectroscopy

sitate normalisation and cleaning prior to cluster analysis [37]. Pareto scaling [38] was performed on PCA models to pre-process the data in order to reduce the influence of higher values and facilitate cluster identification. This approach is common and has been proven to be one of the finest normalisations applied to explore hyperspectral datasets [39]. The score plot, which is a density graph generated by PCA, was used to find clusters characterised by similar spectral signatures. Each dot on the score plot represents a hyperspectral image pixel grouped based on the intensity of the detected variables' values [40]. Image cleaning operations were necessary to improve the interpretation of the initial unreadable models. These procedures were done manually on the PCA itself by selecting and deleting clusters related to portions of the images that were considered irrelevant. This step involved the removal of the background in the hyperspectral image (not relevant for the scope of this study). In the first PCA model, the clustering made it possible to identify and remove outliers due to light reflection and scattering effects. Reflections from external light on the glaze were particularly problematic as they contained no information about the objects' composition and introduced bias in the reading of the PCA models. The image cleaning steps are presented in Online Resource 1. After excluding irrelevant data, the models were reconstructed. The choice of the principal components (PCs) was guided by the ease of recognising high-density clusters associated with distinct pigments in specific regions of the score plot. Different PCs were considered in the score plot to detect the clusters. The resulting PCs were visualised as pseudo-colour images representing the compositional variation as expressed in the corresponding loading lines [40]. The effect of shadows, which created some challenges, was mitigated by deleting the corresponding pixels in the image (through the same image-cleaning protocol described above), although this resulted in gaps in the RGB and false-colour models.

Hyperspectral imaging data were also analysed using ENVI's Spectral Hourglass Wizard (ENVI-SHW) to identify, extract, and map the key image components. Following an initial step of noise reduction through the application of the Savitzky–Golay smoothing filter (13-point window size), SAM (spectral angle mapping) supervised image classification was performed using ENVI 5.0 + IDL software to gain additional insights into the spatial distribution of materials within the dataset. The processing flow implements the minimum noise fraction (MNF) technique to reduce noise and enhance data quality, followed by the isolation of 'spectrally pure' pixels through the Pixel Purity Index (PPI). The n-D Visualizer (a 3D scatter plot) was employed to manually identify the clusters defining the dataset's purest pixels (endmembers). Once the endmembers were extracted, the SAM mapping method visualised their distribution in the image. This algorithm calculates, for each pixel (in radians), the angle between the image's reflectance spectrum and the chosen endmember. A smaller angle indicates a higher spectral similarity. Therefore, pixels were assigned to a specific endmember when the angle was less than or equal to a user-defined tolerance angle. The histogram threshold was manually adjusted for each case to ensure a close match between the spectral characteristics of the identified spatial pixels and the target endmember. The tolerance angle was calculated by averaging the spectra of all pixels assigned to that specific endmember. An acceptable value for the angle was reached when this average closely aligned with the spectral characteristics of the endmember. As a result, the tolerance

angle varied for the hyperspectral cube, ranging from 0.07 to 0.15 radians. Only endmembers representative of the chromophores were selected and investigated. The spectra of the endmembers have been all presented as relative absorbance $\log(1/R)$.

3 Results

The two multivariate analyses tested on the HSI images acquired from the maiolica wares successfully identified repairs, integrations, and restoration parts, when present, and identified the related colouring agents. The spectral characteristics and the identified chromophores for each artefact are summarised in Table 2. When available, XRF data from [33] have also been reported in the table for direct comparison. The images obtained by the PCA with score plots are provided in Online Resource 1, while those obtained by the ENVI-hourglass paradigm coupled with SAM classification are available in Online Resource 2.

3.1 Investigation of maiolica presenting historical restorations

3.1.1 Dish with peacock-eye decoration (1897 M)

The spectral signatures achieved with both the data-processing pipelines allowed to identify the presence of two fully reconstructed parts in the dish with peacock-eye decoration: one in the northern sector of the plate and a smaller one comprising white and orange colours (almost unnoticeable by the naked eye) in the south-eastern sector of the object (Fig. 2). Figure 2a illustrates an example of the absorbance profiles for two white coloured areas (those from the main plate on the left and those from the restored parts on the right) processed by PCA. The extracted endmembers of the white hues appear black in the score plots, and their spatial locations are superimposed in red onto the RGB images to illustrate their distribution. The spectral distinctions obtained in the orange and blue areas further validate the existence of the two restored sections. These results are consistent with the SAM classification, as depicted in the false-colour image in Fig. 2b, where the spatial distributions of the spectral signatures of all colours are shown. White, orange, and blue colours represent endmembers from the main dish, while grey, orange, and light blue indicate the endmembers from the restored part. Absorbance spectra corresponding to each endmember are also provided using the same colour scheme.

Based on the curator's examination of the object, the two integrations evidenced in the HSI images might be made of gypsum plaster. However, this assumption cannot be confirmed since gypsum absorbs in the infrared range. Nevertheless, it is interesting to note that the spectra of all three colours of the two integrations exhibit a consistent absorbance peak at around 710 nm. This absorbance peak, potentially attributed to the $\text{Fe}^{2+}/\text{Ti}^{4+}$ IVCT transition [41, 42], suggests that the two integrations were done using the same material.

Both spectra of the orange hues exhibit a main absorbance at around 450 nm. Despite the main absorbance appearing shifted from what is usually observed in lead antimoniate pigment (~ 440 nm), the observation of a slight shoulder visible at 670 nm might suggest the presence of this pigment in the orange main dish [43]. However, a definitive attribution of the pigment cannot be made in orange areas, and further elemental analysis is required to certainly determine its composition. The spectrum associated with the white restored rim shows an absorbance of around 440 nm, which might be caused by the presence of Fe^{3+} . The white dish spectrum, instead, exhibits a non-attributed peak at around 410 nm. Cobalt oxide has been identified as the primary chromophore for both blue regions, although the two absorbance spectra show some differences. In the blue_dish spectrum, the three characteristic absorption bands of Co^{2+} in tetrahedral coordination (${}^4\text{A}_2(\text{F}) \rightarrow {}^4\text{T}_1(\text{P})$) are identified at around 530 nm, 595 nm, and 645 nm [22, 44, 45]. The blue_restored rim spectrum, on the other hand, exhibits a broad absorption band from 590 to 655 nm, which could be attributed to a combination of cobalt and chromium oxides. The proximity between the absorption peaks of Co^{2+} (595 nm and 645 nm) and Cr^{3+} (650 nm) could have caused an overlap, which added complexity to their investigation and interpretation. Finally, in both the blue areas the presence of iron oxide has been suggested. Both spectra show the absorbance characteristic of ferric cations (~ 440 nm), and the blue restored area also displayed a visible absorbance peak at 900 nm that might be attributed to the dd, spin-allowed ${}^5\text{T}_2 \rightarrow {}^5\text{E}$ transitions of the Fe^{2+} ions in an octahedral site [46].

3.1.2 Pastiche vase with faces in relief (520 M)

Due to the complexity of the object, two hyperspectral images (named HSI_479 and HSI_480) have been acquired to comprehensively examine the vase (Fig. 3). As in the previous object (sample 1897 M), the two data treatments provided equivalent results, aiding in the differentiation and the characterisation of the complex combination of original parts, modern parts, and non-ceramic restoration materials. The object enclosed green, blue, orange, and white–pink areas, which are discussed in detail below. IRFC reflectography improved the recognition of the different parts of the object, as demonstrated by the example of the green sherd of the young, beardless man (IRFC image, HSI_479 in Fig. 3), where three sections can be observed. The upper part of the shirt, which displays a blue–reddish hue, belongs to the same sherd as the neck, classified by the curator as modern. Instead, the two sides of the clothing, which have a darker blue hue, have been previously attributed to original sherds. Finally, the middle part that joins the modern and the original sections is made of non-ceramic material and appears light red in the IRFC image. HSI spectroscopy revealed spectral signatures of distinct materials and colouring agents for these three areas. The examination of the spectra extracted from the

Table 2 Spectral characteristics and chromophores identified in each artefact by hyperspectral imaging spectroscopy

Object	Colour	XRF results [33] (Chromophores)	HSI Results (Chromophores & Spectral Characteristics)
A_AUT1	Green	Cu	Cu ²⁺ (broad absorption 700–900 nm) Fe ³⁺ (440 nm)
	Brown	Mn	Mn ³⁺ (broad spectral band ~490 nm)
B_AUT3	Blue	Co, Fe	Co ²⁺ (530 nm, 595 nm, 654 nm) Fe ³⁺ (440 nm)
	Brown	Mn	Mn ³⁺ (broad spectral band ~490 nm)
B_AUT4	Blue	Co, As	Co ²⁺ (530 nm, 595 nm, 650 nm) Fe ³⁺ (420 nm, 440 nm)
	Orange	Pb, Sb, Fe	Pb ₂ Sb ₂ O ₇ (440 nm, 670 nm) PbO (590 nm) Fe ³⁺ (535 nm)
	Green (aqua)	Cu	Cu ²⁺ (broad absorption 700–900 nm) Fe ³⁺ (425 nm)
	Brown	Mn	Mn ³⁺ (broad spectral band ~490 nm)
C_AUT2	Blue	Co, Bi, Fe	Co ²⁺ (530 nm, 595 nm, 650 nm) Cu ²⁺ (broad absorption 700–900 nm)
581 M	Lustre	Ag, Cu	SPR of silver (443 nm)
	Blue	Co, Mn, Fe	Co ²⁺ (530 nm, 593 nm, 650 nm) Fe ³⁺ (420 nm, 440 nm)
520 M	Lustre	Cu	SPR of silver (440 nm)
	Blue_ORIG (HSI_479 and HSI_480)	nd	Co ²⁺ (530 nm, 597 nm, 650 nm) Fe ³⁺ (440 nm)
	Blue_MOD (HSI_480)	Co, Zn	Co ²⁺ (530 nm, 595 nm, 653 nm)
	Blue_NC (HSI_480)	nd	Co ²⁺ (broad absorbance ~595 nm) Fe ²⁺ /Ti ⁴⁺ (710 nm)
	Orange_ORIG (HSI_479/HSI_480)	Sb, Fe, Cu	Pb ₂ Sb ₂ O ₇ (450 nm and 670 nm)
	Orange_MOD (HSI_480)	Sb, Fe, Cu	Pb ₂ Sb ₂ O ₇ (450 nm and 670 nm)
	Green_ORIG (HSI_479)	Cu, Fe, Sb	Cu ²⁺ (broad absorption 700–900 nm) Fe ³⁺ (440 nm)
	Green_MOD (HSI_479)	Cu, Fe, Co	Co ²⁺ (530, 595 nm, 650 nm) Fe ³⁺ (440 nm)
	Green_NC (HSI_479/HSI_480)	nd	Co ²⁺ (530 nm, broad absorbance 573–640 nm) Fe ³⁺ (440 nm) Fe ²⁺ /Ti ⁴⁺ (710 nm)
	White/pink_ORIG (HIS_479/HIS_480)	nd	Mn ²⁺ (430 nm) Cu ²⁺ (broad absorption 700–900 nm)
	White/pink_MOD (HSI_479)	nd	Mn ²⁺ (435 nm)
	White/pink_NC (HSI_479)	nd	Fe ²⁺ /Ti ⁴⁺ (710 nm)
	Brown_ORIG (HSI_480)	Mn	Mn ³⁺ (broad spectral band ~490 nm)
	Brown_MOD (HSI_479)	Mn, Co	Mn ³⁺ (broad spectral band ~490 nm)
582 M	Blue	Co, Cr, Zn, Mn, Fe	Co ²⁺ (530 nm, 595 nm, 656 nm) Fe ³⁺ (438 nm) Cr ³⁺ (450 nm)

Table 2 continued

Object	Colour	XRF results [33] (Chromophores)	HSI Results (Chromophores & Spectral Characteristics)
	Green	Cu	Cu ²⁺ (broad absorption 700–900 nm)
	Orange	Sb, Fe	Pb ₂ Sb ₂ O ₇ (440 nm, 670 nm) PbO (590 nm) Fe ³⁺ attributable to α-Fe ₂ O ₃ (535 nm)
1897 M	White	–	410 nm
	White_RIM	–	Fe ³⁺ (440 nm) Fe ²⁺ /Ti ⁴⁺ (710 nm)
	Orange	–	Pb ₂ Sb ₂ O ₇ (447 nm, 670 nm)
	Orange_RIM	–	Fe ²⁺ /Ti ⁴⁺ (710 nm)
	Blue	–	Co ²⁺ (530 nm, 595 nm, 645 nm) Fe ³⁺ (440 nm)
	Blue_RIM	–	Fe ²⁺ (900 nm) Fe ³⁺ (440 nm) Co ²⁺ / Cr ³⁺ (broad abs. 590–655 nm) Fe ²⁺ /Ti ⁴⁺ (710 nm)
1838C	Blue	–	Co ²⁺ (530 nm, 595 nm, 655 nm) Fe ³⁺ (438 nm) Cr ³⁺ (450 nm)
	Yellow	–	Pb ₂ Sb ₂ O ₇ (440 nm, 670 nm) PbO (590 nm)
376 M	Green	–	Cu ²⁺ (broad absorption 700–900 nm) Cr ³⁺ (436 nm)
	Yellow	–	PbO (443 nm, 590 nm)
	Brown	–	Mn ³⁺ (broad spectral band ~490 nm)

XRF data from [33] have also been reported when available. nd = not detected; – = not analysed; ORIG = original; MOD = modern; NC = non-ceramic

green area of the original sherds comprising the two sides of the shirt (HSI_479_green_ORIG) suggests a copper-based colour. The chromophore identification is based on a broad absorbance band between 750 and 900 nm, attributed to the ${}^2E_g \rightarrow {}^2T_{2g}$ transition of the Cu²⁺ octahedral complex [47]. This band is a consequence of the transition being split into sub-bands, mainly due to distortions in the site along the z-axis. It arises from the overlap and combination of two resulting electronic transitions, ${}^2B_{1g} \rightarrow {}^2A_{1g}$ and ${}^2B_{1g} \rightarrow {}^2E_g$, resulting in a broad and asymmetric band [48]. Furthermore, the ferric cation absorbance has been observed (~440 nm); even if iron oxide has not been considered the primary chromophore, it may have contributed to the green/yellow hue [49]. The XRF analysis conducted on the pastiche agrees with these findings since it identified copper and iron, in addition to trace amounts of antimony, which were not highlighted by HIS. Absorption peaks characteristic of iron and cobalt oxides have been detected in the spectrum of the modern green sherd (HSI_479_green_MOD); the latter is most likely the cause of the reddish hue observed for this area in the IRFC [20]. The elemental analysis confirmed the presence of these metal oxides, revealing also the presence of copper, non-detected by HSI, potentially due to its presence at trace levels. The spectra of the non-ceramic green integration collected in both HSI images (HSI_479_green_NC and HSI_480_green_NC) are equivalent. Moreover, they feature a similar composition to green_MOD, consisting of iron and cobalt oxides. This latter is suggested by the broad absorption range at 573–640 nm and the peak detected at 532 nm in HSI_480_green_NC. Noteworthy is the 710 nm absorbance peak, already observed in the non-ceramic integrations of sample 1897 M, which has been associated with iron and titanium (elements confirmed by XRF data). The differences in chemical compositions between these green regions provide compelling evidence that the different sherds composing the object are indeed made of distinct materials and chromophores, which confirms that this is an assemblage of parts made in different moments, as previously reported. It is possible that the ceramists who produced the modern sherds added cobalt oxide in addition to copper oxides to match the original green hue. The majority of the faces of the two characters come from the same original sherd. Both white/pink_ORIG spectra (HSI_479 for the beardless man and HSI_480 for the bearded man) appear similar. Despite the noise of the spectra, an absorbance peak around 430 nm, particularly visible in the HSI_480_ORIG spectrum, suggests the presence of manganese cations. Additionally, a broad absorbance at around 900 nm, especially noticeable in the HSI_479_ORIG spectrum, indicates the presence of cupric cations, potentially explaining the bluish appearance of the faces in the IRFC image. This hue is also observable in the facial fragment attached to the young man's hair (IRFC HSI_479); this similarity, together with the correspondence of their spectral features, confirms that they are matching original sherds. The spectrum representing the neck of the young man in the modern sherd (HSI_479_white/pink_MOD) only shows an absorbance peak at 435 nm, which, despite being slightly shifted,

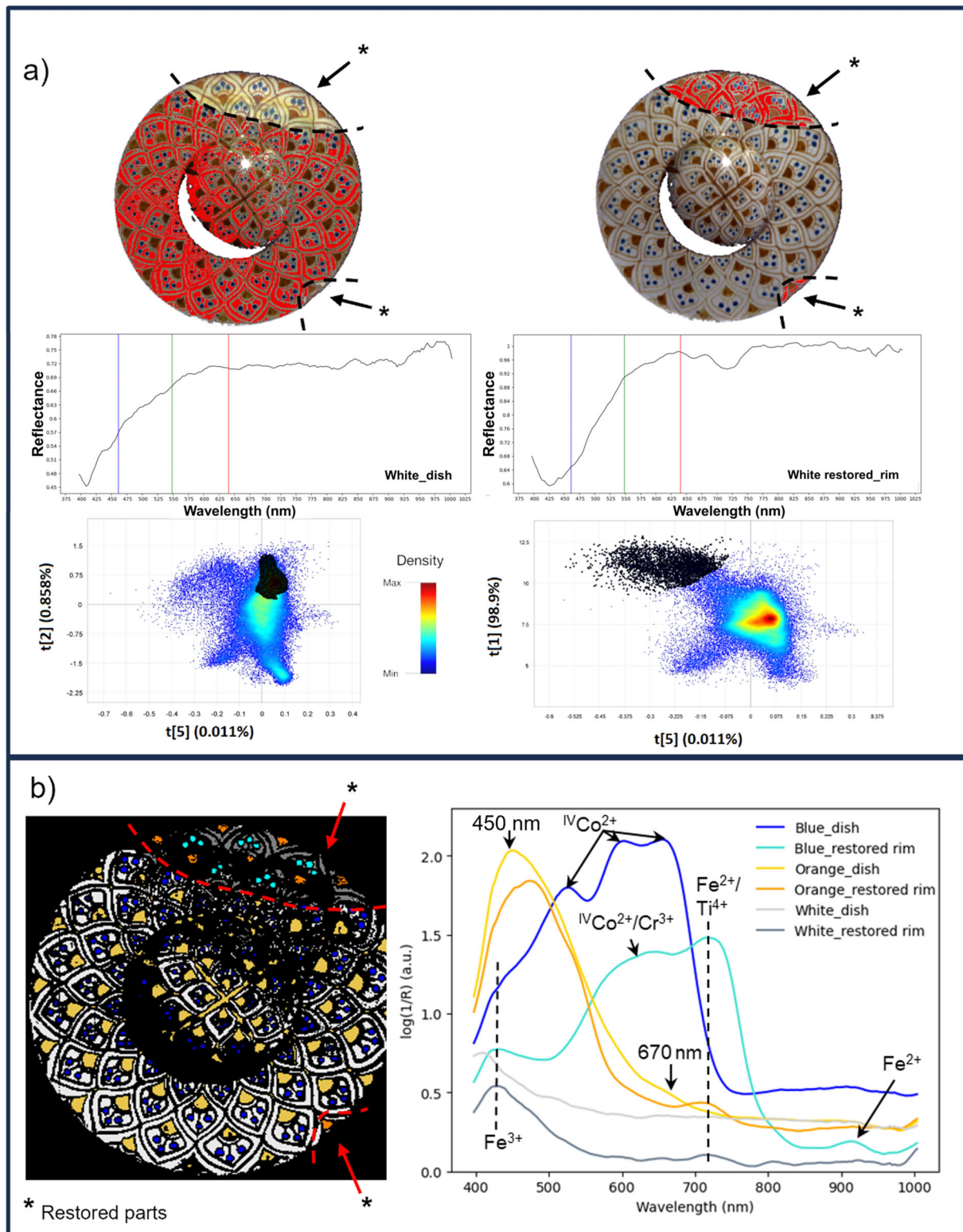


Fig. 2 Results obtained from the dish with peacock-eye decoration (1897 M) with the two data treatment pipelines. **a** PCA score plots (where the highest density is indicated by the colour red, followed by the colours orange, yellow, green, light blue and blue), spectra and RGB images illustrating the two different white colours present in the artefact. The score plot selection of the extracted endmembers is highlighted in black, along with the corresponding region in the RGB image marked in red. The left side results correspond to the main part of the plate, while the right side is representative of the two restored parts in the rim. **b** Classification performed with the SAM algorithm (left) and the absorbance spectra of the extracted endmembers for each hue (right)

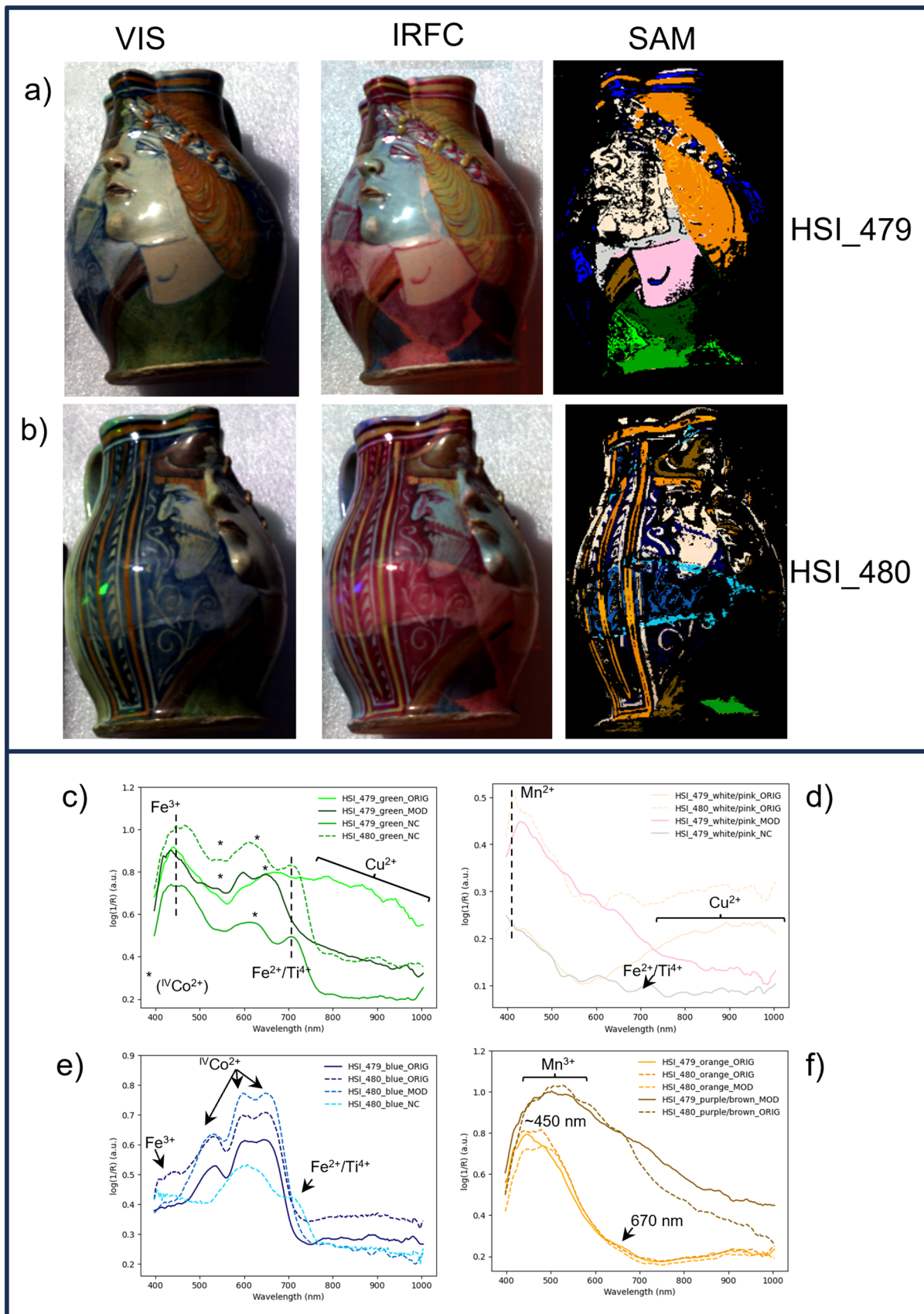


Fig. 3 Hyperspectral imaging in RGB, IRFC and SAM classification of *pastiche* vase with faces in relief 520 M: **a** HSI_479 and **b** HSI_480. Absorbance spectra of the extracted endmembers: **c** green, **d** white/rose, **e** blue, **f** yellow and brown. Dashed lines in the graphs correspond to H_480 endmembers, while solid lines depict HSI_479 data

can be associated with Mn^{2+} . Finally, the non-ceramic material used to join original and modern sherds, represented as grey in the SAM classification (HSI_479_white/pink_NC), is characterised by the absorbance peak attributable to $\text{Fe}^{2+}/\text{Ti}^{4+}$ IVCT transition.

In the VIS and IRFC images of HSI_480, it is possible to discriminate a sherd in the middle, comprising blue and orange shades. This sherd has been characterised as modern. Despite their distinct visual appearance, especially in the IRFC image (more reddish hue), the spectral properties of these colours closely resemble those of the original sherds, suggesting the use of similar colouring agents. Regarding the blue areas, cobalt oxide has been detected in both original and modern sherds. Precisely, the triplet characteristic of Co^{2+} is visible in the spectra of the upper part near the bearded man (HSI_480_blue_ORIG), the hairband of the young man (HSI_479_blue_ORIG) and the modern sherd in the middle (HSI_480_blue_MOD). An absorbance attributable to ferric cations (440 nm) in the HSI_480_blue_ORIG spectrum might suggest the trace presence of iron in the original blue recipe. XRF analysis confirmed the presence of cobalt in the blue of the original sherds but not in the modern one. The spectrum of the blue area of the non-ceramic material used to join the sherds (HSI_480_blue_NC), alongside the consistently present peak at 710 nm ($\text{Fe}^{2+}/\text{Ti}^{4+}$), shows a broad absorbance at around 595 nm, which might suggest the presence of cobalt oxide in trace amounts. The analysis also determined the use of a similar colouring agent for the orange colouration in the original and modern sherds. Specifically, similar absorbance features have been observed from the orange upper part near the bearded man (HSI_480_orange_ORIG), the hair of the young man (HSI_479_orange_ORIG), and the modern sherd in the middle (HSI_480_orange_MOD). Similarly to the orange spectrum of the sample 1897 M, all spectra display a prominent absorbance peak around 450 nm and a minor shoulder at 670 nm, which might be attributed to a lead antimoniate pigment. This interpretation was supported by the Sb content determined through XRF. The elemental analysis also detected Fe, whose absorbance signal was not observed. Iron could explain the orange hue, which aligns with other studies on Italian maiolica [24, 50].

Finally, purple-brown linear decorations are visible in the pastiche vase in both HSI_479 and HSI_480 images. The spectrum collected from HSI_479 belongs to the modern sherd with the young man's neck (purple/brown_MOD), while the spectrum from HSI_480 belongs to an original sherd located on the right of the lower sherd (purple/brown_ORIG). As the orange and blue hues, the original and modern brown colourations appear to be obtained using the same colouring agent: manganese oxide. Both absorbance spectra show a broad band at around 490 nm, characteristic of the d-d electronic transition of the manganese ion Mn^{3+} [22]. Previous elemental analysis [33] corroborated the presence of consistent chromophores for orange, blue and brown areas in the original and the modern sherds (Table 2). However, it is crucial to note that XRF indicated a significant difference between original and modern pieces, the latter having a notably higher concentration of zinc. This was not discernible from HSI data.

3.2 Identification of the colouring agents

The study then moved to the characterisation of the chromophores in all the other studied items, with the results summarised in Table 2. The objective was to understand the colour palette and determine the authenticity of the objects of unknown origin that had not been examined before.

3.2.1 Blues

The spectroscopic study revealed the use of cobalt as the primary colouring agent for the blue hue of all the maiolica artefacts, including original samples (B_AUT3, C_AUT2, B_AUT4, 581 M), forgeries (582 M), and objects of uncertain authenticity (1838 C). In Fig. 4, all the spectra show the typical Co^{2+} triplet at around 530 nm, 595 nm and 650 nm. In the artefacts 582 M, B_AUT3, and 1838C, a sharp peak around 440 nm, attributed to Fe^{3+} , has been observed. Furthermore, in the tile with lustred decoration (581 M) and in the sample B_AUT4, an additional peak at 420 nm, also ascribed to trivalent iron, was highlighted [47, 51]. A broader absorbance around 800 nm in the spectrum of C_AUT2, attributable to Cu^{2+} transitions, suggests the presence of copper oxide. Since ancient times, copper and cobalt ores have been widely used in the blue colouration of glasses and ceramics. Co-doped glasses exhibit hues with an intense blue, which can be toned down by adding copper oxide (CuO).

Interestingly, samples 1838C and 582 M show a significant peak at approximately 450 nm, attributed to Cr^{3+} transitions (${}^4\text{A}_{2g} \rightarrow {}^4\text{T}_1$ (F)) [20, 52]. The presence of chromium, responsible for the greenish hue and previously confirmed through XRF on the jar (582 M), supports the modern origin of these objects since chromium emerged as a prominent ceramic dye particularly after 1802. Although the presence of chromium in some mediaeval green enamels has been attributed to the use of chromium-bearing Bohemian garnet [53], its presence in these maiolica strongly suggests their nineteenth-century origin.

3.2.2 Yellows, oranges and lustres

The yellow and orange hues in samples C_AUT2 and 581 M are identified as lustres, characterised by a peak at around 443 nm, indicative of the surface plasmon resonance (SPR) band of silver absorption [23] (Fig. 5). Lustre is a refined decorative technique used in maiolica, which involves the application on the glaze of a thin metallic film mainly composed of silver and copper. This meticulous process produces iridescent reflections in various colours, ranging from bright yellow to orange and red, depending on particle dimensions and/or the percentage of copper and silver [50]. Comparison with XRF analysis (Table 2) reveals the presence of both copper and silver colloidal metal particles. The exclusive detection of silver absorption is not unexpected: in a system

Fig. 4 Absorbance spectra of blue regions of original samples (B_AUT3, C_AUT2, B_AUT4, 581 M), forgeries (582 M), and objects of uncertain authenticity (1838C)

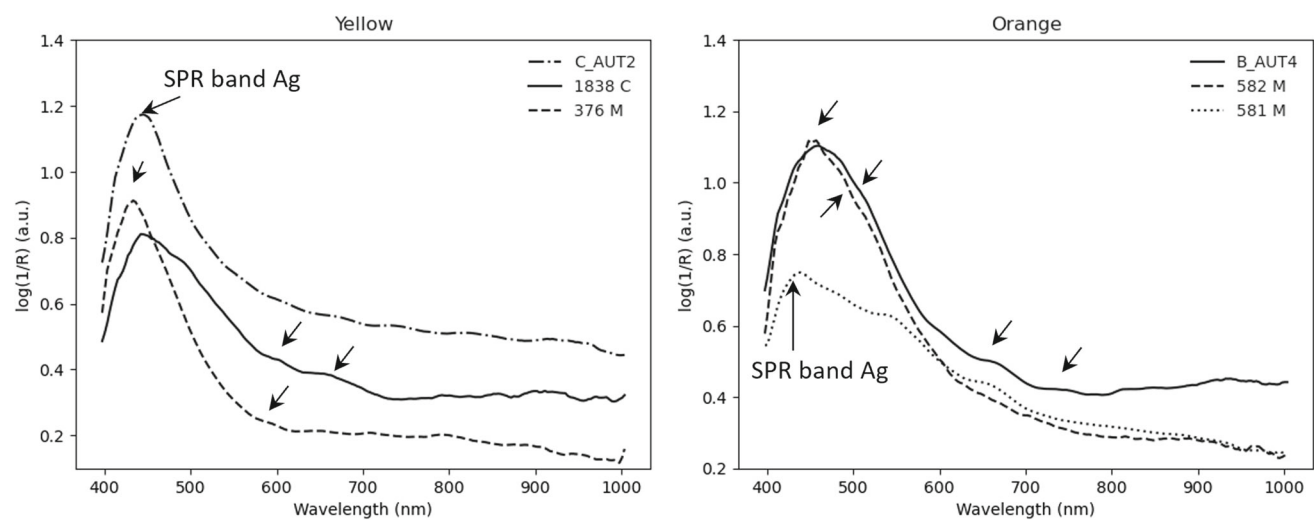
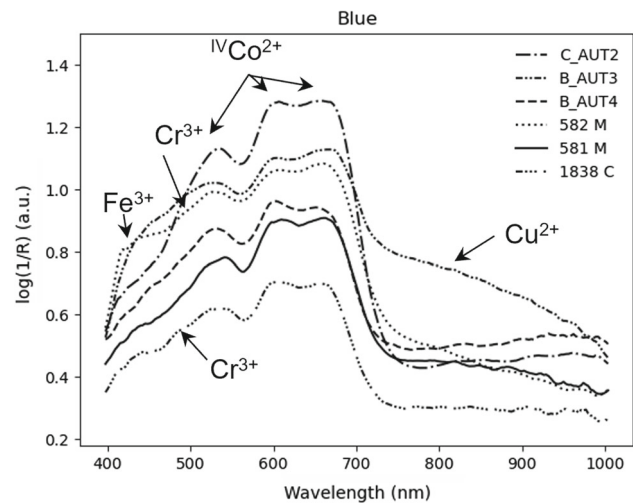


Fig. 5 Absorbance spectra of (left) yellow regions in original samples (C_AUT2) and objects of uncertain authenticity (1838C, 376 M), and (right) orange regions in original samples (B_AUT4, 581 M) and forgeries (582 M)

containing both copper and silver nanoparticles, the SPR characteristics observed by HSI may primarily reflect the properties of the silver nanoparticles if they predominate in number or exhibit distinctive SPR behaviour due to their size or shape. While copper nanoparticles may contribute to the overall optical response of the system, they may not exhibit strong SPR characteristics within the spectral range of interest.

The yellow and orange hues in samples 1838C, B_AUT4, and 582 M are ascribed to the lead antimoniate pigment ($\text{Pb}_2\text{Sb}_2\text{O}_7$) thanks to the distinctive absorption peaks at around 440 nm and 670 nm. The shoulder at 590 nm might be assigned to PbO [43] suggesting the co-presence of the two compounds. The slight peak at 535 nm in the samples B_AUT4 and 582 M might be due to the six coordinated Fe^{3+} of crystalline hematite ($\alpha\text{-Fe}_2\text{O}_3$) [43]. XRF analysis performed on these two samples confirmed the presence of lead, antimony, and iron. Finally, the presence of only two bands at 443 nm and 590 nm in the yellow shades of sample 376 M might suggest the use of a yellow pigment containing lead (potentially PbO).

3.2.3 Greens

All samples displaying green colouring exhibit broad absorbance with a maximum of around 800 nm, characteristic of Cu^{2+} (Fig. 6, left). While 582 M (forgery) appears to have only copper as a chromophore, B_AUT4 and A_AUT1 (original sherds) show peaks attributable to Fe^{3+} (425 nm and 440 nm). The greenish-blue appearance observed in sample 376 M, whose origin is uncertain, might be characterised by a combination of chromium and copper oxides. This suggestion is prompted by the sharp absorbance peak at 436 nm, possibly the Cr^{3+} peak, typically at 450 nm, but shifted to a shorter wavelength in the presence of copper. The presence of chromium oxide would imply a potential modern (post-nineteenth century) origin for the dish with deer decoration (376 M). However, further analysis is required to substantiate this hypothesis.

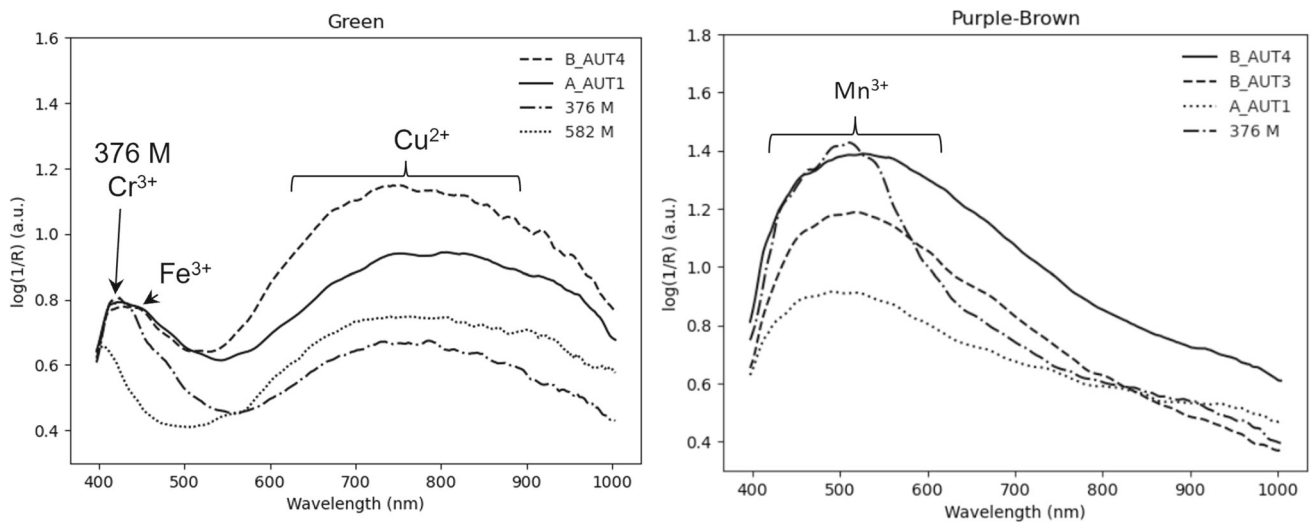


Fig. 6 Absorbance spectra of (left) green regions in original samples (B_AUT4, A_AUT1), forgeries (582 M), and objects of uncertain authenticity (376 M); (right) brown regions in original samples (B_AUT4, B_AUT3, A_AUT1), and objects of uncertain authenticity (376 M)

3.2.4 Purple-browns

The purple-brown colourations observed in samples B_AUT4, B_AUT3, A_AUT1, and 376 M can be attributed to manganese-based pigments. These pigments exhibit a broad absorbance band at approximately 490 nm, a characteristic feature of Mn^{3+} ions (Fig. 6, right). In glazes, where manganese is a colouring agent, Mn^{2+} and Mn^{3+} ions coexist, and their equilibrium determines the resulting colour. The electronic transitions of Mn^{2+} ions have low probabilities due to spin and parity restrictions, resulting in weak absorption and a yellowish or minimally coloured appearance. On the other hand, the manganic ion Mn^{3+} in octahedral coordination allows for spin-allowed d-d transitions, leading to strong absorption in the visible range, typically at 470–520 nm. This spectral band displays broad asymmetry due to energy level splitting caused by the Jahn–Teller distortion [49]. Moreover, atmospheric conditions during firing influence manganese's behaviour. In highly oxidising atmospheres, manganese primarily exists as Mn^{3+} , resulting in a purple colouration, as in the case of the objects analysed in this study. Conversely, the manganese would predominantly appear as Mn^{2+} in a reducing atmosphere, yielding a lighter yellow–brown colour.

4 Discussion and conclusions

This study demonstrated the suitability and effectiveness of an ultraportable HSI camera in examining highly refractive and three-dimensional glazed maiolica wares within the constraints of a museum environment, with rapid acquisition times and in a non-invasive way. The methodology yielded valuable information for reconstructing the production techniques of the studied artefacts (e.g. the colouring agents used for decoration), as well as the restoration and integration work carried out over time. After acquiring a single image of the artefact, a data mining approach can be applied, and different information can be extracted. The HSI analyses conducted on two artefacts, a dish with peacock-eye decoration (1897 M) and a pastiche vase with faces in relief (520 M), revealed evidence of integrations and restorations by identifying distinct compositions within each object. Spectroscopic analysis confirmed that the pastiche vase comprises five distinct sherds from two different periods. Original sherds depict, for example, the faces, hair, and fragments of a shirt, while modern additions include the necks and chins. The use of different colouring agents enabled the differentiation of the sherds, particularly in green regions where cobalt was identified in the modern ones, while only copper was present in the original ones. Original white/pink sherds showed absorbance from copper in addition to manganese, unlike the modern ones. While the HSI data did not directly indicate which sherds were modern and which were original, it validated assumptions when combined with stylistic analysis and prior XRF compositional analysis. For instance, it aided in attributing various sherds to the same group, as in the case of the two sherds portraying the face and hair of a beardless man. The comparison between HSI and previous XRF results highlighted the significance of employing a comprehensive and multi-analytical approach. Hyperspectral data offered additional and complementary insights, including the determination of the chemical compositions of the chromophores (e.g. the valence of ions) and the characterisation of pigments such as lead antimoniate. The spectroscopic analysis, however, faced challenges in differentiating between original and modern parts in the blue, orange, and brown areas due to the presence of similar chromophores, whereas XRF revealed that modern parts had higher zinc concentrations. Interestingly, the presence of Co in the original blue areas was identified by HSI but not by XRF. This is probably due to the concentration of cobalt, which is typically very low in glasses and glazes [45, 54]. Cobalt is easily detected optically, even when present in trace amounts, thanks to its significantly

higher linear absorption coefficient, approximately five times larger than that of other metal oxides [52, 55]. Regarding the non-ceramic integrations introduced during restoration, both the maiolica wares (1897 M and 520 M) exhibited an absorbance peak at 710 nm, indicative of both iron and titanium presence, consistent with the XRF findings on the pastiche 520 M. The presence of the same peak in the integrations of both objects suggests that similar restoration materials were used even though they were probably restored in different periods. Furthermore, the detection of chromium in the blue integration of dish 1897 M implies its post-nineteenth-century production.

HSI spectroscopy also made it possible to identify the main colouring agents in all the samples analysed, which are those typical of the Italian maiolica technique: cobalt in the blues, copper in the greens, manganese in the purple-browns, silver in the lustres and lead antimonate pigments in the yellows, with the addition of iron-based pigments in the oranges (Table 2). Chromium, not typically documented in medieval or Renaissance maiolica, was detected in the blues of pharmacy jar 582 M (a forgery) and leopard figurine 1838C (of unknown origin), as well as in the greens of the bowl with deer 376 M (also of unknown origin). The presence of chromium suggests a production period around or after the nineteenth century when chromium-based pigments became prevalent. This finding is particularly significant for objects 1838C and 376 M, previously unanalysed, indicating they are likely to be modern forgeries. On the contrary, in the case of the dish with peacock-eye decoration 1897 M (i.e. the other object with uncertain origin analysed), it was not possible to either confirm or refute its authenticity. In some cases, the presence of additional ions and the consequent different spectroscopic signatures led to the discernment of colours having similar appearances to the naked eye, as in the case of the different cobalt-based blues.

Two HSI data processing methods, namely PCA with score plots and the ENVI-hourglass paradigm coupled with SAM classification, were tested to extract optimal information under flawed lighting conditions. Despite the variations in concepts and function, both pipelines provided equivalent results, independently leading to the identification of the same integrations and chromophores. From a methodological point of view, the choice of approach should be guided by the study's goals while considering the possibilities and limitations of the two methods. To optimise the analysis, a suggested procedure could involve using PCA initially for comprehensive sample screening, detecting outliers and anomalies, and then using SAM to map the different spectral elements.

The findings derived from HSI on maiolica hold significant implications for curators and museum professionals. They furnish scientific evidence pivotal in identifying past restoration treatments and shed light on the authenticity of artefacts, especially in cases where historical documentation is scant or previous restorations remain undocumented. Furthermore, these techniques offer invaluable assistance to archaeologists and art historians in delineating the production methods employed in crafting maiolica, as well as elucidating the alterations the objects underwent over time. To maximise the efficacy of this method, it is imperative to expand the existing database of HSI absorbance spectra for coloured glazes.

Supplementary Information The online version contains supplementary material available at <https://doi.org/10.1140/epjp/s13360-024-05405-7>.

Acknowledgements The authors warmly thank Dr Marino Marini, curator of the Museo Nazionale del Bargello, for providing access to the collection and precious information on the analysed objects.

Funding Open access funding provided by Università degli Studi di Firenze within the CRUI-CARE Agreement. This study received financial support from the French government in the framework of the University of Bordeaux's IdEx 'Investments for the Future' programme/GPR 'Human Past'. The University of Bordeaux Montaigne, the CNRS and the University of Pisa are also acknowledged. The open-access publication costs have been covered by the University of Florence.

Data Availability Statement This manuscript has data included as electronic supplementary material. [Author's comment: The authors declare that the data supporting the findings of this study are available in the paper's supplementary information files. The raw data are available on request from the authors.]

Declarations

Conflict of interest The authors have no conflicts of interest to declare that are relevant to the content of this article.

Open Access This article is licensed under a Creative Commons Attribution 4.0 International License, which permits use, sharing, adaptation, distribution and reproduction in any medium or format, as long as you give appropriate credit to the original author(s) and the source, provide a link to the Creative Commons licence, and indicate if changes were made. The images or other third party material in this article are included in the article's Creative Commons licence, unless indicated otherwise in a credit line to the material. If material is not included in the article's Creative Commons licence and your intended use is not permitted by statutory regulation or exceeds the permitted use, you will need to obtain permission directly from the copyright holder. To view a copy of this licence, visit <http://creativecommons.org/licenses/by/4.0/>.

References

1. C. Sciuto, F. Cantini, R. Chapoulie, C. Cou, H. De la Codre, G. Gattiglia, X. Granier, A. Mounier, V. Palleschi, G. Sorrentino, S. Raneri, What lies beyond sight? Applications of ultraportable hyperspectral imaging (VIS-NIR) for archaeological fieldwork. *J. Field Archaeol.* **47**, 522–535 (2022). <https://doi.org/10.1080/00934690.2022.2135066>
2. M. Picollo, C. Cucci, A. Casini, L. Stefani, Hyper-spectral imaging technique in the cultural heritage field: new possible scenarios. *Sensors* **20**, 2843 (2020). <https://doi.org/10.3390/s20102843>

3. L. Liu, T. Miteva, G. Delnevo, S. Mirri, P. Walter, L. de Viguierie, E. Pouyet, Neural networks for hyperspectral imaging of historical paintings: a practical review. *Sensors* **23**, 2419 (2023). <https://doi.org/10.3390/s23052419>
4. M. Vermeulen, K. Smith, K. Eremin, G. Rayner, M. Walton, Application of uniform manifold approximation and projection (UMAP) in spectral imaging of artworks. *Spectrochim. Acta. A. Mol. Biomol. Spectrosc.* **252**, 119547 (2021). <https://doi.org/10.1016/j.saa.2021.119547>
5. T. Kleyhans, D.W. Messinger, J.K. Delaney, Towards automatic classification of diffuse reflectance image cubes from paintings collected with hyperspectral cameras. *Microchem. J.* **157**, 104934 (2020). <https://doi.org/10.1016/j.microc.2020.104934>
6. F. Daniel, A. Mounier, Mobile hyperspectral imaging for the non-invasive study of a mural painting in the Belves Castle (France, 15th C). *STAR Sci. Technol. Archaeol. Res.* **1**, 81–88 (2015). <https://doi.org/10.1080/20548923.2016.1183942>
7. C. Cucci, M. Picollo, L. Chiarantini, G. Uda, L. Fiori, B. De Nigris, M. Osanna, Remote-sensing hyperspectral imaging for applications in archaeological areas: non-invasive investigations on wall paintings and on mural inscriptions in the Pompeii site. *Microchem. J.* **158**, 105082 (2020). <https://doi.org/10.1016/j.microc.2020.105082>
8. F. Gabrieli, K.A. Dooley, M. Facini, J.K. Delaney, Near-UV to mid-IR reflectance imaging spectroscopy of paintings on the macroscale. *Sci. Adv.* **5**, eaaw7794 (2019). <https://doi.org/10.1126/sciadv.aaw7794>
9. M. Pérez, E. Arroyo-Lemus, J.L. Ruvalcaba-Sil, A. Mitrani, M.A. Maynez-Rojas, O.G. de Lucio, Technical non-invasive study of the novo-hispanic painting the Pentecost by Baltasar de Echave Orrio by spectroscopic techniques and hyperspectral imaging: in quest for the painter's hand. *Spectrochim. Acta. A. Mol. Biomol. Spectrosc.* **250**, 119225 (2021). <https://doi.org/10.1016/j.saa.2020.119225>
10. H.D.L. Codre, F. Daniel, R. Chapoulie, L. Servant, A. Mounier, Investigating the materials used in eighteenth-century tapestries from the three French Royal Manufactories: inputs of hyperspectral approaches. *Eur. Phys. J. Plus* **136**, 1193 (2021). <https://doi.org/10.1140/epjp/s13360-021-02184-3>
11. P. Claisse, H. De La Codre, W. Nowik, F. Daniel, R. Chapoulie, M. Dallel, A. Mounier, Original and restored materials revealed by contactless and micro-invasive methods of the Lady and the Unicorn tapestry “Mon seul désir.” *Eur. Phys. J. Plus* **138**, 832 (2023). <https://doi.org/10.1140/epjp/s13360-023-04435-x>
12. I.J. Maybury, D. Howell, M. Terras, H. Viles, Comparing the effectiveness of hyperspectral imaging and Raman spectroscopy: a case study on Armenian manuscripts. *Herit. Sci.* **6**, 42 (2018). <https://doi.org/10.1186/s40494-018-0206-1>
13. V. Biolcati, M. Wilson, S. Fiddly, R. Unitt, C.C. Ryan, A.G. Hoffmann, J. Gillis, F. France, P.Ó. Macháin, D. Iacopino, The book of Uí Mhaine: an interdisciplinary analysis of the materiality of the Gaelic manuscript tradition. *Heritage* **6**, 5393–5409 (2023). <https://doi.org/10.3390/heritage6070284>
14. A. Mounier, G. Le Bourdon, C. Aupetit, S. Lazare, C. Biron, J. Pérez-Arategui, D. Almazán, J. Aramendia, N. Prieto-Taboada, S. Fdez-Ortiz de Vallejuelo, F. Daniel, Red and blue colours on 18th–19th century Japanese woodblock prints: In situ analyses by spectrofluorimetry and complementary non-invasive spectroscopic methods. *Microchem. J.* **140**, 129–141 (2018). <https://doi.org/10.1016/j.microc.2018.04.023>
15. M.L. Clarke, F. Gabrieli, K.L. Rowberg, A. Hare, J. Ueda, B. McCarthy, J.K. Delaney, Imaging spectroscopies to characterize a 13th century Japanese handscroll, The Miraculous Interventions of Jizō Bosatsu. *Herit. Sci.* **9**, 20 (2021). <https://doi.org/10.1186/s40494-021-00497-1>
16. O. Yatsuk, G. Fiocco, M. Malagodi, A. Re, A. Lo Giudice, C. Iaia, M. Gulmini, The non-invasive characterization of iron age glass finds from the “Gaetano Chierici” collection in Reggio Emilia (Italy). *Heritage* **6**, 5583–5606 (2023). <https://doi.org/10.3390/heritage6070294>
17. A. Babini, P. Green, S. George, J.Y. Hardeberg, Comparison of hyperspectral imaging and fiber-optic reflectance spectroscopy for reflectance and transmittance measurements of colored glass. *Heritage* **5**, 1401–1419 (2022). <https://doi.org/10.3390/heritage5030073>
18. C. Jones, C. Duffy, A. Gibson, M. Terras, Understanding multispectral imaging of cultural heritage: determining best practice in MSI analysis of historical artefacts. *J. Cult. Herit.* **45**, 339–350 (2020). <https://doi.org/10.1016/j.culher.2020.03.004>
19. C. Cucci, A. Casini, L. Stefani, M. Picollo, J. Jussila, Bridging research with innovative products: a compact hyperspectral camera for investigating artworks: a feasibility study, in: *Opt. Arts Archit. Archaeol. VI, SPIE*, 2017: pp. 17–29. <https://doi.org/10.1117/12.2270015>
20. E. Beauvoit, A. Amara, R. Chapoulie, Q. Lemasson, A multianalytical approach for the study of relief polychrome glazed ceramics (France, 19th century). *J. Archaeol. Sci. Rep.* **51**, 104176 (2023). <https://doi.org/10.1016/j.jasrep.2023.104176>
21. C. Meucci, L. Carratoni, Identification of the majolica polychromatic decoration by IRFC methodology. *J. Archaeol. Sci. Rep.* **8**, 224–234 (2016). <https://doi.org/10.1016/j.jasrep.2016.06.027>
22. M. Aceto, G. Fenoglio, M. Labate, M. Picollo, M. Bacci, A. Agostino, A fast non-invasive method for preliminary authentication of mediaeval glass enamels using UV–visible–NIR diffuse reflectance spectrophotometry. *J. Cult. Herit.* **45**, 33–40 (2020). <https://doi.org/10.1016/j.culher.2020.05.003>
23. G. Padeletti, P. Fermo, How the masters in Umbria, Italy, generated and used nanoparticles in art fabrication during the Renaissance period. *Appl. Phys. Mater. Sci. Process.* **76**, 515–525 (2003). <https://doi.org/10.1007/s00339-002-1935-1>
24. M. Gulmini, F. Scognamiglio, G. Roselli, G. Vaggelli, Composition and microstructure of maiolica from the museum of ceramics in Ascoli Piceno (Italy): evidences by electron microscopy and microanalysis. *Appl. Phys. A* **120**, 1643–1652 (2015). <https://doi.org/10.1007/s00339-015-9376-9>
25. D. Bersani, L. Saviane, A. Morigi, L. Mantovani, M. Aceto, L. Fornasini, Multi-technique characterization of glass mosaic tesserae from Villa di Teodorico in Galeata (Italy). *J. Raman Spectrosc.* **52**, 2234–2245 (2021). <https://doi.org/10.1002/jrs.6180>
26. E. Balliana, E.M.C. Caveri, L. Falchi, E. Zendri, Tiles from Aosta: a peculiar glaze roof covering. *Colorants* **2**, 533–551 (2023). <https://doi.org/10.3390/colorants2030026>
27. M.S. Tite, The production technology of Italian maiolica: a reassessment. *J. Archaeol. Sci.* **36**, 2065–2080 (2009). <https://doi.org/10.1016/j.jas.2009.07.006>
28. S.L. Niece, Restoration, pastiche and fakes, in: *Radiogr. Cult. Mater*, 2nd ed., Routledge, (2005).
29. L. Frescobaldi Malenchini, *Il Risorgimento della maiolica italiana : Ginori e Cantagalli = The Revival of Italian Maiolica : Ginori and Cantagalli*, (2011) 9–357.
30. M. Marini, Il commercio di ceramiche antiche (e falsi) a Firenze fra '800 e '900, Falsi E Copie Nella Maiolica Mediev. E Mod. Model. Tec. Diffus. *Gusto Riconoscibilità* (2017) 107–125. <https://doi.org/10.1400/253410>
31. R. Manca, Non-invasive, scientific analysis of 19th-century gold jewellery and maiolica. A contribution to technical art history and authenticity studies. *Plinius* **47**, 36–42 (2021). <https://doi.org/10.19276/plinius.2021.01006>
32. P. Craddock, *Scientific Investigation of Copies* (Taylor & Francis, Fakes and Forgeries, 2009)
33. R. Manca, E. Tartaglia, C. Ruberto, M. Marini, L. Chiarantini, A. Gueli, S. Pasquale, M. Chiari, S.E. Mangani, P.A. Mandò, F. Taccetti, M. Benvenuti, Studio di autenticazione di alcune maioliche del Museo Nazionale del Bargello: Il contributo delle analisi scientifiche, in “LV Convegno Internazionale della Ceramica – Lo studio della ceramica nel 2022. Metodologie e case studies,” Cent. Ligure Storia Della Ceram. Ed. All’Insegna Giglio Firenze ISBN 9788892852457 E-ISBN 9788892852464 ISBN 9788892852457 Pp 167–179 (2023).
34. S. Baronti, A. Casini, F. Lotti, S. Porcinai, Principal component analysis of visible and near-infrared multispectral images of works of art. *Chemom. Intell. Lab. Syst.* **39**, 103–114 (1997). [https://doi.org/10.1016/S0169-7439\(97\)00047-6](https://doi.org/10.1016/S0169-7439(97)00047-6)
35. S. Legnaioli, G. Lorenzetti, G.H. Cavalcanti, E. Grifoni, L. Marras, A. Tonazzini, E. Salerno, P. Pallecchi, G. Giachi, V. Pallecchi, Recovery of archaeological wall paintings using novel multispectral imaging approaches. *Herit. Sci.* **1**, 33 (2013). <https://doi.org/10.1186/2050-7445-1-33>

36. G. Gattiglia, M. Puntin, C. Sciuto, Archeologie dell'invisibile. Tecniche archeometriche non distruttive per la caratterizzazione dei laterizi del sito romano di Massaciuccoli. *Riv. Archeol.* **46**, 125–146 (2022)
37. P. Geladi, H. Isaksson, L. Lindqvist, S. Wold, K. Esbensen, Principal component analysis of multivariate images. *Chemom. Intell. Lab. Syst.* **5**, 209–220 (1989). [https://doi.org/10.1016/0169-7439\(89\)80049-8](https://doi.org/10.1016/0169-7439(89)80049-8)
38. R.A. van den Berg, H.C. Hoefsloot, J.A. Westerhuis, A.K. Smilde, M.J. van der Werf, Centering, scaling, and transformations: improving the biological information content of metabolomics data. *BMC Genom.* **7**, 142 (2006). <https://doi.org/10.1186/1471-2164-7-142>
39. M. Song, S. Liu, D. Xu, H. Yu, Multiobjective optimization-based hyperspectral band selection for target detection. *IEEE Trans. Geosci. Remote Sens.* **60**, 1–22 (2022). <https://doi.org/10.1109/TGRS.2022.3176856>
40. H.F. Grahn, P. Geladi (eds.), *Techniques and Applications of Hyperspectral Image Analysis*, 1st edn. (Wiley, 2007). <https://doi.org/10.1002/9780470010884>
41. M.N. Taran, Electronic intervalence $\text{Fe}^{2+} + \text{Ti}^{4+} \rightarrow \text{Fe}^{3+} + \text{Ti}^{3+}$ charge-transfer transition in ilmenite. *Phys. Chem. Miner.* **46**, 839–843 (2019). <https://doi.org/10.1007/s00269-019-01044-y>
42. M. Aceto, E. Calà, F. Gulino, F. Gullo, M. Labate, A. Agostino, M. Picollo, The use of UV-visible diffuse reflectance spectrophotometry for a fast, Preliminary authentication of gemstones. *Molecules* **27**, 4716 (2022). <https://doi.org/10.3390/molecules27154716>
43. G. Padeletti, P. Fermo, S. Gilardoni, A. Galli, Technological study of ancient ceramics produced in Casteldurante (central Italy) during the Renaissance. *Appl. Phys. A* **79**, 335–339 (2004). <https://doi.org/10.1007/s00339-004-2521-5>
44. M. Bacci, M. Picollo, Non-destructive spectroscopic detection of cobalt(II) in paintings and glass. *Stud. Conserv.* **41**, 136–144 (1996). <https://doi.org/10.1179/sic.1996.41.3.136>
45. A. Ceglie, W. Meulebroeck, K. Baert, H. Wouters, K. Nys, H. Thienpont, H. Terryn, Cobalt absorption bands for the differentiation of historical Na and Ca/K rich glass. *Surf. Interface Anal.* **44**, 219–226 (2012). <https://doi.org/10.1002/sia.3810>
46. L. De Ferri, R. Arletti, G. Ponterini, S. Quartieri, XANES, UV-VIS and luminescence spectroscopic study of chromophores in ancient HIMT glass. *Eur. J. Mineral.* **23**, 969–980 (2011). <https://doi.org/10.1127/0935-1221/2011/0023-2125>
47. C. Cherian, L. de Ferri, G. Pojana, R. Falcone, A. Cianciosi, S. Gelichi, Preliminary non-invasive study of Roman glasses from Jesolo (Venice), Italy. *Glass Technol. Eur. J. Glass Sci. Technol. Part A* **61**(1), 1–15 (2020). <https://doi.org/10.13036/17533546.61.1.003>
48. D. Möncke, M. Papageorgiou, A. Winterstein-Beckmann, N. Zacharias, Roman glasses coloured by dissolved transition metal ions: redox-reactions, optical spectroscopy and ligand field theory. *J. Archaeol. Sci.* **46**, 23–36 (2014). <https://doi.org/10.1016/j.jas.2014.03.007>
49. A. Paul, Coloured Glasses, in *Chemistry of Glasses*, ed. by A. Paul (Springer Netherlands, Dordrecht, 1982), pp.204–276. https://doi.org/10.1007/978-94-009-5918-7_7
50. S. Padovani, I. Borgia, B. Brunetti, A. Sgamellotti, A. Giulivi, F. D'Acapito, P. Mazzoldi, C. Sada, G. Battaglin, Silver and copper nanoclusters in the lustre decoration of Italian Renaissance pottery: an EXAFS study. *Appl. Phys. A* **79**, 229–233 (2004). <https://doi.org/10.1007/s00339-004-2516-2>
51. A. Ceglie, G. Nuyts, W. Meulebroeck, S. Cagno, A. Silvestri, A. Zoleo, K. Nys, K. Janssens, H. Thienpont, H. Terryn, Iron speciation in soda-lime-silica glass: a comparison of XANES and UV-vis-NIR spectroscopy. *J. Anal. At. Spectrom.* **30**, 1552–1561 (2015). <https://doi.org/10.1039/C5JA00046G>
52. W. Meulebroeck, H. Wouters, K. Nys, H. Thienpont, Authenticity screening of stained glass windows using optical spectroscopy. *Sci. Rep.* **6**, 37726 (2016). <https://doi.org/10.1038/srep37726>
53. I.C. Freestone, M. Bimson, The possible early use of chromium as a glass colorant. *J. Glass Stud.* **45**, 183–185 (2003)
54. E. Gliozzo, A. Santagostino Barbone, F. D'Acapito, M. Turchiano, I. Turbanti Memmi, G. Volpe, The sectilia panels of faragola (ascoli Satriano, Southern Italy): a multi-analytical study of the green, marbled (green and Yellow), Blue and Blackish Glass Slabs. *Archaeometry* **52**, 389–415 (2010). <https://doi.org/10.1111/j.1475-4754.2009.00493.x>
55. J. Henderson, *Ancient Glass: An Interdisciplinary Exploration* (Cambridge University Press, Cambridge, 2013)